Composites: Part B 55 (2013) 247–262

Contents lists available at SciVerse ScienceDirect

Composites: Part B

journal homepage: www.elsevier.com/locate/compositesb

Numerical analysis of square reinforced concrete plates strengthened by fiber-reinforced plastics with various patterns

Cindrawaty Lesmana, Hsuan-Teh Hu *, Fu-Ming Lin, Nan-Ming Huang

Department of Civil Engineering, National Cheng Kung University, Tainan 701, Taiwan, ROC

ARTICLE INFO

Article history:
Received 18 April 2012
Received in revised form 24 April 2013
Accepted 12 June 2013
Available online 27 June 2013

Keywords:
A. Plates
C. Finite element analysis
A. Laminates

ABSTRACT

Abaqus finite element program is employed to analyze the ultimate load capacities of square reinforced concrete plates strengthened by fiber-reinforced plastics. Appropriate constitutive models are introduced and validated to stimulate nonlinear material behavior of reinforced concrete and fiber-reinforced plastics. The influences of FRP reinforcement, steel reinforcement, and concrete properties on the ultimate strengths of the reinforced concrete plates are investigated. Finally, based on the numerical results, empirical equations are proposed to predict increment of ultimate load capacities of the square reinforced concrete plates strengthened by fiber-reinforced plastics, which would be useful for practical engineering applications.

1. Introduction

Due to the high strength-to-weight ratio, high durability, and good resistance to corrosion and fatigue, fiber-reinforced plastic (FRP) has replaced the traditional strengthening material, steel, and been intensively used in the strengthening of reinforced concrete (RC) structures in recent years. In addition, FRP can be simply installed since there are no requirements for laps and joints. They can take up irregularities in the shapes of concrete surfaces and have no problems with overlapping due to the thinness of the materials [1].

The research on the FRP to strengthen the RC structures has been started on the characteristics of material behavior [2], the interface between RC and FRP [3–5], the performance and failure of the composite materials and members [6–9]. As the result, different technologies of strengthening have been developed on the purposes of increasing the load carrying capacities of RC structures.

Performances of RC structures with bonded external FRP have been studied by many researchers experimentally [7,10,11] and numerically [12–14]. However, only a few investigators conducted the study for RC plates strengthened by FRPs. In many research work, the behavior of FRP was assumed to be linear [12,15] but unidirectional fibrous composites exhibit severe nonlinearity in their in-plane shear stress–strain relations [16]. In addition, deviation from linearity is also observed with in-plane transverse loading but the degree of nonlinearity is not comparable to that observed with the in-plane shear [16,17]. In order to accurately predict the load carrying capacities of RC structures strengthened by FRPs, the nonlinear behavior of FRP should be modeled properly [18].

In this investigation, proper constitutive models are introduced to simulate the nonlinear behavior of concrete and FRP. These material constitutive models are validated with the experiment data of Mosallam and Mosalam [10] using Abaqus finite element program [19]. Then, extensive numerical analyses are carried out to analyze the ultimate load capacities of square reinforced concrete plates strengthened by FRP. In addition, the influences of fiber orientations and various strengthening patterns of FRP on the ultimate strengths of the reinforced concrete plates are investigated. Finally, based on the numerical results, empirical equations are proposed to predict the ultimate load capacities of the square reinforced concrete plates strengthened by FRP, which would be useful for practical engineering applications.

2. Constitutive models of material

The materials used in the analysis involve steel reinforcing bars, concrete and FRP. Reliable constitutive models applicable to steel reinforcing bars and concrete are available in the Abaqus material library. Thus, their input material properties and associated constitutive models are briefly introduced. Since the Abaqus program does not have a nonlinear material library for FRP, its nonlinear constitutive model is discussed here in detail. The consequential nonlinear constitutive equations for the FRP are coded in FORTRAN language as a subroutine and linked to the Abaqus program.

* Corresponding author. Tel.: +886 6 2757575x63168; fax: +886 6 2358542.
E-mail address: hthu@mail.ncku.edu.tw (H.-T. Hu).

1359-8368/$ - see front matter © 2013 Elsevier Ltd. All rights reserved.
http://dx.doi.org/10.1016/j.compositesb.2013.06.021

2.1. Steel reinforcing bar

The elastic modulus of the steel reinforcement is assumed to be

$$E_s = 200\ \text{GPa} \tag{1}$$

The elastic perfectly plastic is assumed to exemplify the stress–strain curve of the reinforcing bar.

2.2. Concrete

The Poisson's ratio v_c of concrete under uniaxial compressive stress ranges from 0.15 to 0.22, with a representative value of 0.19 or 0.20 [20]. In this study, the Poisson's ratio of concrete is assumed to be

$$v_c = 0.2 \tag{2}$$

Let the uniaxial compressive strength and the corresponding strain of the concrete be f_c' and ε_o. The value of ε_o is usually around the range of 0.002–0.003. A representative value suggested by ACI Committee 318 [21] and used in the analysis is

$$\varepsilon_o = 0.003 \tag{3}$$

The uniaxial tensile strength f_t' of concrete is difficult to measure. For this study the value is taken as [20]

$$f_t' = 0.33\sqrt{f_c'}\ \text{MPa} \tag{4}$$

The initial modulus of elasticity of concrete E_c is highly correlated to its compressive strength and can be calculated with reasonable accuracy from the empirical equation [1].

$$E_c = 4700\sqrt{f_c'}\ \text{MPa} \tag{5}$$

Under multiaxial combinations of loading, the failure strengths of concrete are different from those observed under uniaxial condition. However, the maximum strength envelope under multiple stress conditions seems to be largely independent of load path [22]. In Abaqus, a Mohr–Coulomb type compression surface together with a crack detection surface is used to model the failure surface of concrete (Fig. 1). When the principal stress components of concrete are in biaxial compression zone, the response of the concrete is modeled by an elastic–plastic theory with an associated flow and an isotropic hardening rule. When the principal stress components of concrete are in biaxial tension zone or in biaxial tension–compression zone, cracking of concrete is defined to occur by the crack detection surface. Once cracking of concrete takes place, the orientation of the crack is stored. Damaged elasticity is then used to model the existing crack [19].

When plastic deformation occurs, there should be a certain parameter to guide the expansion of the yield surface. A commonly used approach is to relate the multidimensional stress and strain conditions to a pair of quantities, namely, the effective stress σ_c and effective strain ε_c, such that results obtained following different loading paths can all be correlated by means of the equivalent uniaxial stress–strain curve. The stress–strain relationship proposed by Saenz [23] has been widely adopted as the uniaxial stress–strain curve for concrete and it has the following form

$$\sigma_c = \frac{E_c\varepsilon_c}{1 + (R + R_E - 2)\left(\frac{\varepsilon_c}{\varepsilon_o}\right) - (2R-1)\left(\frac{\varepsilon_c}{\varepsilon_o}\right)^2 + R\left(\frac{\varepsilon_c}{\varepsilon_o}\right)^3} \tag{6}$$

where

$$R = \frac{R_E(R_\sigma - 1)}{(R_\varepsilon - 1)^2} - \frac{1}{R_\varepsilon}, \quad R_E = \frac{E_c}{E_o}, \quad E_o = \frac{f_c'}{\varepsilon_o}$$

and $R_\sigma = 4$, $R_\varepsilon = 4$ will be used [24]. In the analysis, Eq. (6) is taken as the equivalent uniaxial stress–strain curve for concrete and approximated by several piecewise linear segments inputted to Abaqus.

When cracking of concrete takes place, a smeared model is used to represent the discontinuous macro crack behavior. It is known that the cracked concrete of a RC element can still carry some tensile stress in the direction normal to the crack, which is termed tension stiffening [20]. In this study, a simple descending line is used to model this tension stiffening phenomenon (Fig. 2). The default value of the strain ε^* at which the tension stiffening stress reduced to zero is [4]

$$\varepsilon^* = 0.001 \tag{7}$$

During the post cracking stage, the cracked RC can still transfer shear forces through aggregate interlock or shear friction, which is termed shear retention. Assuming that the shear modulus of intact concrete is G_c, then the reduced shear modulus $\widehat{G}$ of cracked concrete can be expressed as

$$\widehat{G} = \mu G_c \tag{8}$$

$$\mu = (1 - \varepsilon/\varepsilon_{\max}) \tag{9}$$

where ε is the strain normal to the crack direction and $\varepsilon_{\max}$ is the strain at which the parameter μ reduces to zero. Numerous analytical results have demonstrated that the particular value chosen for μ (between 0 and 1) does not appear to be critical but values greater than zero are necessary to prevent numerical instabilities [23,25]. In

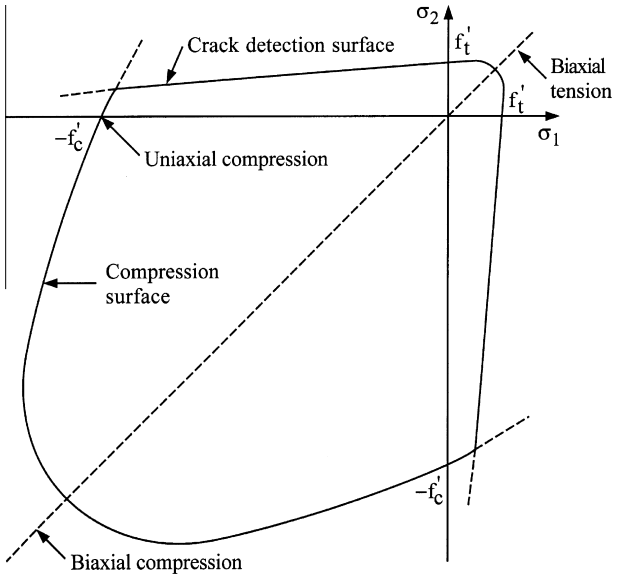

Fig. 1. Concrete failure surface in plane stress.

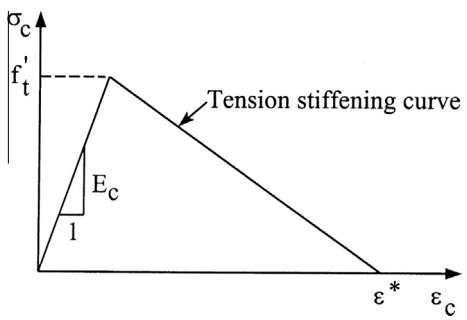

Fig. 2. Tension stiffening model.

Abaqus, ε_{max} is usually assumed to be a very large value, i.e., $\mu = 1$ (full shear retention). In this investigation, the default values for tension stiffening parameter $\varepsilon^* = 0.001$ and for shear retention parameter $\mu = 1$ are used.

2.3. Fiber-reinforced plastics

For FRP (Fig. 3), each lamina can be considered as an orthotropic layer in a plane stress condition. It is well known that unidirectional fibrous composites exhibit severe nonlinearity in their in-plane shear stress–strain relation. In addition, deviation from linearity is also observed with in-plane transverse loading but the degree of nonlinearity is not comparable to that in the in-plane shear [16]. Usually, this nonlinearity associated with the transverse loading can be ignored [20]. To model the nonlinear in-plane shear behavior, the nonlinear strain–stress relation for a composite lamina suggested by Hahn and Tsai [17] is adopted as follows:

$$\begin{Bmatrix} \varepsilon_1 \\ \varepsilon_2 \\ \gamma_{12} \end{Bmatrix} = \begin{bmatrix} \frac{1}{E_{11}} & -\frac{\nu_{21}}{E_{22}} & 0 \\ -\frac{\nu_{12}}{E_{11}} & \frac{1}{E_{22}} & 0 \\ 0 & 0 & \frac{1}{G_{12}} \end{bmatrix} \begin{Bmatrix} \sigma_1 \\ \sigma_2 \\ \tau_{12} \end{Bmatrix} + S_{6666}\tau_{12}^2 \begin{Bmatrix} 0 \\ 0 \\ \tau_{12} \end{Bmatrix} \tag{10}$$

In this model only one constant S_{6666} is required to account for the in-plane shear nonlinearity. The value of S_{6666} can be determined by a curve fit to various off-axis tension test data [16]. Let us define $\Delta\{\sigma'\} = \Delta\{\sigma_1, \sigma_2, \tau_{12}\}^T$ and $\Delta\{\varepsilon'\} = \Delta\{\varepsilon_1, \varepsilon_2, \gamma_{12}\}^T$. Inverting and differentiating Eq. (10), the incremental stress–strain relations are established

$$\Delta\{\sigma'\} = [Q_1']\Delta\{\varepsilon'\} \tag{11}$$

$$[Q_1'] = \begin{bmatrix} \frac{E_{11}}{1-\nu_{12}\nu_{21}} & \frac{\nu_{12}E_{22}}{1-\nu_{12}\nu_{21}} & 0 \\ \frac{\nu_{21}E_{11}}{1-\nu_{12}\nu_{21}} & \frac{E_{22}}{1-\nu_{12}\nu_{21}} & 0 \\ 0 & 0 & \frac{1}{1/G_{12}+3S_{6666}\tau_{12}^2} \end{bmatrix} \tag{12}$$

Furthermore, it is assumed that the transverse shear stresses always behave linearly and do not affect the nonlinear behavior of any in-plane shear. If we define $\Delta\{\tau_t'\} = \Delta\{\tau_{13}, \tau_{23}\}^T$ and $\Delta\{\gamma_t'\} = \Delta\{\gamma_{13}, \gamma_{23}\}^T$, the constitutive equations for transverse shear stresses become

$$\Delta\{\tau_t'\} = [Q_2']\Delta\{\gamma_t'\} \tag{13}$$

$$[Q_2'] = \begin{bmatrix} \alpha_1 G_{13} & 0 \\ 0 & \alpha_2 G_{23} \end{bmatrix} \tag{14}$$

where α_1 and α_2 are the shear correction factors and are taken to be 0.83 in this study.

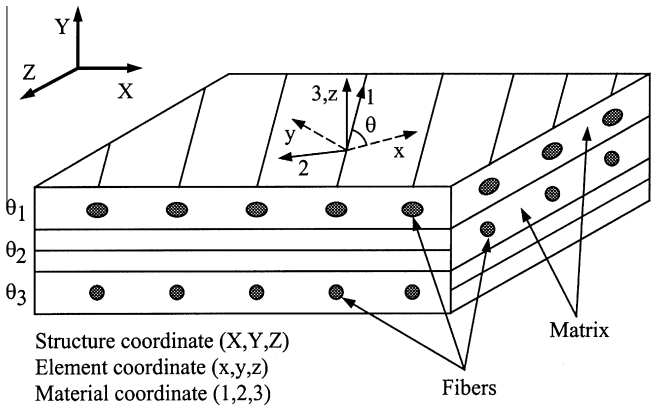

Fig. 3. Material, element and structure coordinates of fiber reinforced plastics.

Among existing failure criteria, the Tsai-Wu criterion [26] has been extensively used in the literature and is adopted in this analysis. Under plane stress conditions, this failure criterion has the following form

$$F_1\sigma_1 + F_2\sigma_2 + F_{11}\sigma_1^2 + 2F_{12}\sigma_1\sigma_2 + F_{22}\sigma_2^2 + F_{66}\tau_{12}^2 = 1 \tag{15}$$

with

$$F_1 = \frac{1}{\overline{X}} + \frac{1}{\overline{X}'}, \quad F_2 = \frac{1}{\overline{Y}} + \frac{1}{\overline{Y}'}, F_{11} = \frac{-1}{\overline{X}\overline{X}'}, F_{22} = \frac{-1}{\overline{Y}\overline{Y}'}, F_{66} = \frac{1}{\overline{S}^2}.$$

The $\overline{X}$, $\overline{Y}$ and $\overline{X}'$, $\overline{Y}'$ are the lamina longitudinal and transverse strengths in tension and compression, respectively, and $\overline{S}$ is the shear strength of the lamina. Though the stress interaction term F_{12} in Eq. (15) is difficult to be determined, it has been suggested that F_{12} can be set equal to zero for practical engineering applications [27]. Therefore, $F_{12} = 0$ is used in this investigation.

During the numerical calculation, incremental loading is applied to composite plates until failures in one or more of individual plies are indicated according to Eq. (15). Since the Tsai-Wu criterion does not distinguish failure modes, the following two rules are used to determine whether the ply failure is caused by resin fracture or fiber breakage [28]:

(1) If a ply fails but the stress in the fiber direction remains less than the uniaxial strength of the lamina in the fiber direction, i.e. $\overline{X}' < \sigma_1 < \overline{X}$, the ply failure is assumed to be resin induced. As a result, the laminate loses its capability to support transverse and shear stresses, but remains to carry longitudinal stress. In this case, the constitutive matrix of the lamina becomes

$$[Q_1'] = \begin{bmatrix} E_{11} & 0 & 0 \\ 0 & 0 & 0 \\ 0 & 0 & 0 \end{bmatrix} \tag{16}$$

(2) If a ply fails with σ_1 exceeding the uniaxial strength of the lamina, the ply failure is caused by the fiber breakage and a total ply rupture is assumed. In this case, the constitutive matrix of the lamina becomes

$$[Q_1'] = \begin{bmatrix} 0 & 0 & 0 \\ 0 & 0 & 0 \\ 0 & 0 & 0 \end{bmatrix} \tag{17}$$

During a FE analysis, the constitutive matrix of composite materials at the integration points of shell elements must be calculated before the stiffness matrices are assembled from the element level to the structural level. For composite materials, the incremental constitutive equations of a lamina in the element coordinates (x, y, z) can be written as:

$$\Delta\{\sigma\} = [Q_1]\Delta\{\varepsilon\} \tag{18}$$

$$\Delta\{\tau_t\} = [Q_2]\Delta\{\gamma_t\} \tag{19}$$

where $\Delta\{\sigma\} = \Delta\{\sigma_x, \sigma_y, \tau_{xy}\}^T$, $\Delta\{\tau\} = \Delta\{\tau_{xz}, \tau_{yz}\}^T$, $\Delta\{\varepsilon\} = \Delta\{\varepsilon_x, \varepsilon_y, \gamma_{xy}\}^T$, $\Delta\{\gamma\} = \Delta\{\gamma_{xz}, \gamma_{yz}\}^T$, and

$$[Q_1] = [T_1]^T[Q_1'][T_1] \tag{20}$$

$$[Q_2] = [T_2]^T[Q_2'][T_2] \tag{21}$$

$$[T_1] = \begin{bmatrix} \cos^2\theta & \sin^2\theta & \sin\theta\cos\theta \\ \sin^2\theta & \cos^2\theta & -\sin\theta\cos\theta \\ -2\sin\theta\cos\theta & 2\sin\theta\cos\theta & \cos^2\theta - \sin^2\theta \end{bmatrix} \tag{22}$$

$$[T_2] = \begin{bmatrix} \cos\theta & \sin\theta \\ -\sin\theta & \cos\theta \end{bmatrix} \tag{23}$$

The θ is measured counterclockwise from the element local x-axis to the material 1-axis (Fig. 5). Let $\Delta\{\varepsilon_o\} = \Delta\{\varepsilon_{xo}, \varepsilon_{yo}, \varepsilon_{xyo}\}^T$ be the incremental in-plane strains at the mid-surface of the shell section and $\Delta\{\kappa\} = \Delta\{\kappa_x, \kappa_y, \kappa_{xy}\}^T$ the incremental curvatures. The incremental inplane strains at a distance z from the mid-surface of the shell section become

$$\Delta\{\varepsilon\} = \Delta\{\varepsilon_o\} + z\Delta\{\kappa\} \tag{24}$$

Let h be the total thickness of the composite shell section, the incremental stress resultants, $\Delta\{N\} = \Delta\{N_x, N_y, N_{xy}\}^T$, $\Delta\{M\} = \Delta\{M_x, M_y, M_{xy}\}^T$ and $\Delta\{V\} = \Delta\{V_x, V_y\}^T$ can be defined as

$$\begin{Bmatrix} \Delta\{N\} \\ \Delta\{M\} \\ \Delta\{V\} \end{Bmatrix} = \int_{-h/2}^{h/2} \begin{Bmatrix} \Delta\{\sigma\} \\ z\Delta\{\sigma\} \\ \Delta\{\tau_t\} \end{Bmatrix} dz \tag{25}$$

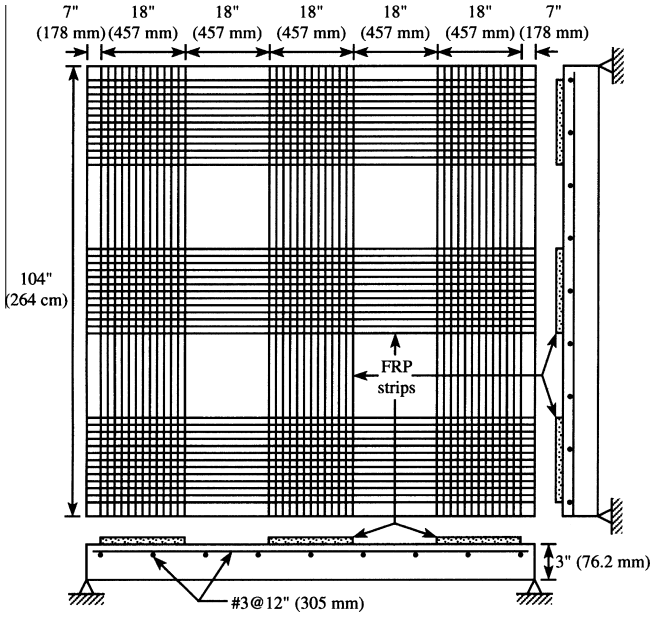

Fig. 4. Mosallam–Mosalam specimens for reinforced concrete square plate [10].

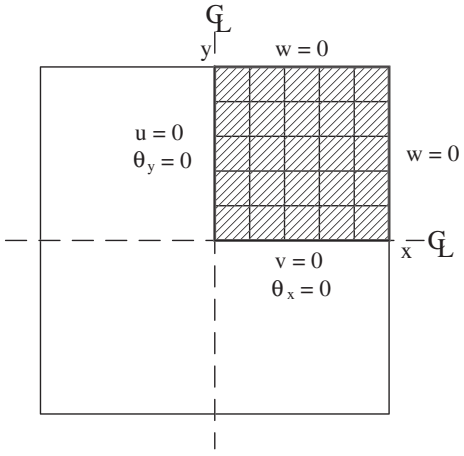

Fig. 5. Boundary condition assumption for Mosallam–Mosalam specimens in FE analysis.

Substituting Eqs. (18), (19) and (24) into the above expression, one can obtain the stiffness matrix for the fiber composite laminate shell at the integration point as

$$\begin{Bmatrix} \Delta\{N\} \\ \Delta\{M\} \\ \Delta\{V\} \end{Bmatrix} = \int_{-h/2}^{h/2} \begin{bmatrix} [Q_1] & z[Q_1] & [0] \\ z[Q_1] & z^2[Q_1] & [0] \\ [0]^T & [0]^T & [Q_2] \end{bmatrix} \begin{Bmatrix} \Delta\{\varepsilon_o\} \\ \Delta\{\kappa\} \\ \Delta\{\gamma_t\} \end{Bmatrix} dz \tag{26}$$

where [0] is a 3 by 2 null matrix.

3. Verification of the proposed material constitutive models

The validity of the material models for steel and FRP had been verified individually by testing against experimental data [19,29] and is not duplicated here. This section demonstrates the validity of these material models to simulate the behavior of purely RC plate and RC plate strengthened by FRP, respectively. In the numerical analyses, the Newton stabilize method [19] in Abaqus was used to carry out the nonlinear FE solutions. The method is appropriate for producing a stable result in the stiffened structure [30].

For verification purpose, two square RC plates tested by Mosallam and Mosalam [10] were studied. As shown in Fig. 4, the clear span of the plates in both directions is 264 cm with a constant thickness of 76.2 mm. The plates were simply supported at the four edges and were subjected to a uniform static pressure applied to the bottom surface of the plates up to failure. The compressive strength f'_c of concrete was 32.87 MPa. Both of the RC plates were fabricated using Grade 60 reinforcing steel with the yielding strength σ_y equals to 413.7 MPa. Tension (top) reinforcement consisted of #3 rebar (9.5 mm diameter) at 305 mm equal spacing in the two orthogonal directions of each plate with 13 mm cover. While one specimen was purely RC plate, the other specimen was strengthened by two FRP layers spaced at 457 mm and adhered to the top side with their fiber directions oriented in the two orthogonal directions of the plate (Fig. 4). At the intersection regions of the staggered unidirectional laminates, bidirectional fiber architecture, i.e. [90/0/90/0] lamination layup, was formed. Each FRP layer was 0.58 mm in thickness with tensile strength $\overline{X} = 1209$ MPa and modulus $E_{11} = 101$ GPa. Due to limited experimental data, the following parameters were assumed: $v_{12} = 0.3$, $\overline{X}' = -1209$ MPa, $\overline{Y} = 12$ MPa, $\overline{Y}' = -12$ MPa, $\overline{S} = 12$ MPa, $E_{22} = 1$ GPa, and $G_{12} = 1$ GPa. In addition, a maximum strain criterion, i.e. $\varepsilon_1 \leqslant 0.008$ [27], was used together with the Tsai-Wu criterion for FRP in this numerical analysis.

The plates had two planes of symmetry. To reduce the cost of analysis, only 1/4 portion of the plates were analyzed as shown from hatch area in Fig. 5. Accordingly, symmetric boundary conditions were placed along the two symmetric planes. The finite element mesh had 25 reinforced concrete shell elements in total (5 rows in each FRP strip direction) and eight-node quadrilateral shell elements with reduced integration rule were used to model the RC plates. The fiber-reinforced plastics were also modeled by the eight-node quadrilateral shell elements with reduced integration rule. In the numerical analysis, it was assumed that there is no slip between the steel, concrete, and FRP [18]. For plate strengthened with FRP strips, 21 FRP shell elements were used.

Fig. 6 shows the total lateral force versus vertical displacement at the center of the purely RC plate as well as the strengthened plate. It can be observed that the correlations are very good between numerical results and experimental data for both specimens. For purely reinforced concrete plate, the predicted ultimate load, 219.8 kN, is very close to the experimental result, 219.3 kN, so the error percentage is only 0.23%. The predicted ultimate load for strengthened plate is the same as the experimental data, 434.3 kN. Those results confirm the proposed material constitutive models are justified to be able to simulate the composite behavior of the

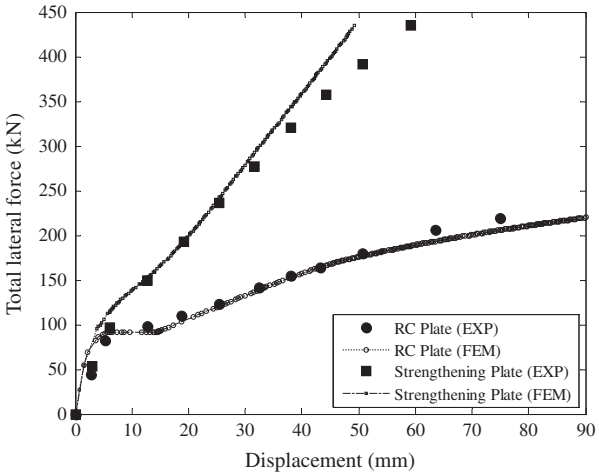

Fig. 6. Load–displacement curves of RC square plates with and without FRP based on Mossalam's plate.

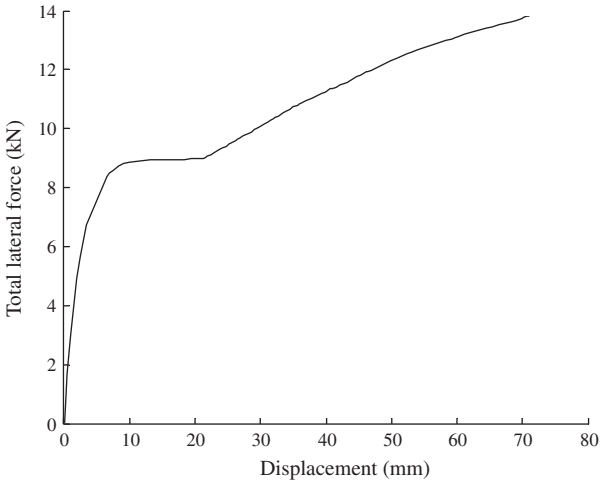

Fig. 8. Load–displacement curve of RC square plates subjected to concentrated load.

plates correctly. In addition, we can find that due to the contribution of FRP, the ultimate load of the reinforced concrete plate is significantly increased by 98%. This proves the usefulness of FRP to strengthen the RC structures.

4. Numerical analysis

The numerical models were generated similar with the plate's dimension of the experimental worked in Fig. 4. To evaluate various factors that affect FRP as external reinforcement for RC plates, four aspect factors of tensile strengthening were pointed out, i.e.: location of FRP, percentage area of FRP to the plate, number of layers, and fiber angle of lamina. The numerical analyses also conduct to observe some factors on matrix of composite plates, i.e.: concrete properties, steel reinforcement ratios, and subjected load (distributed load and concentrated load). In this analysis, the strengthening patterns limited to three types as illustrated in Fig. 7. Type 1 (Fig. 7a) is the composite plates with square shape of FRP localized at center of the plate. Type 2 (Fig. 7b) is the composite plates with FRP strip located along diagonal of plate. Type 3 (Fig. 7c) is the composite plates with diamond shape of FRP localized at center of the plate.

To observe the effects of adhered FRP into load capacity of the strengthened plates, each pattern was analyzed with different cases of FRP ratio. FRP ratio (%FRP) calculates as the ratio between the surface area of plate that adhered by FRP and the total area of the RC plate. Five different FRP ratios as shown in Fig. 7 were elaborated for type 1 (4%, 16%, 36%, 64%, and 100%) and type 3 (2%, 8%, 18%, 32%, and 50%), whereas four cases were formed for type 2 (19%, 36%, 64%, and 84%). The analysis also generated in evaluating

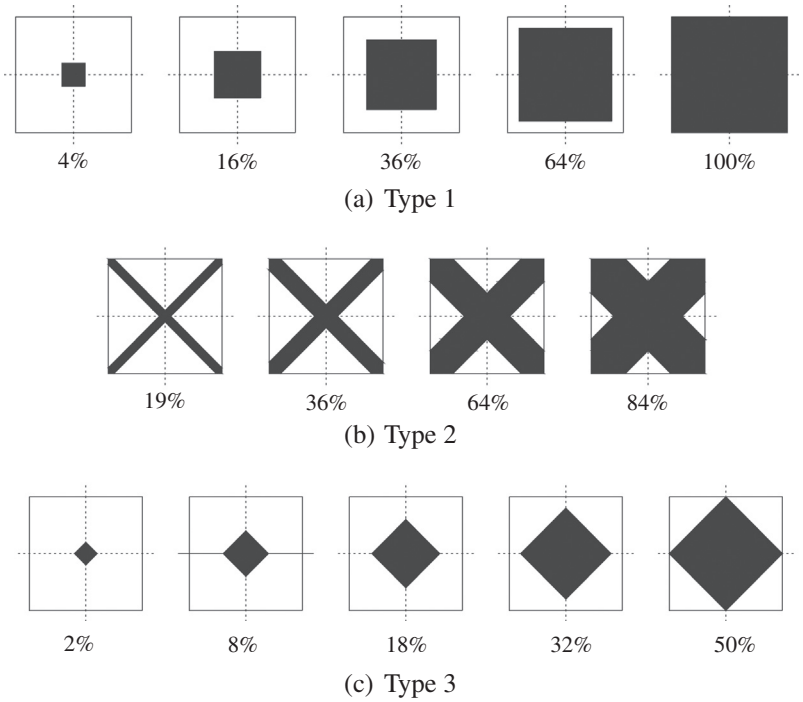

Fig. 7. Strengthening types of composite RC square plates.

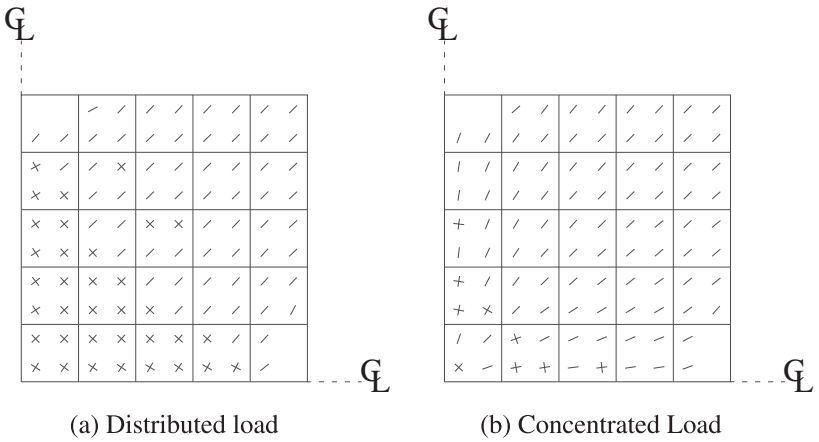

Fig. 9. Crack pattern for RC square plate for $f_c' = 32.87$ MPa and $\rho_s = 0.0037$ due to subjected load.

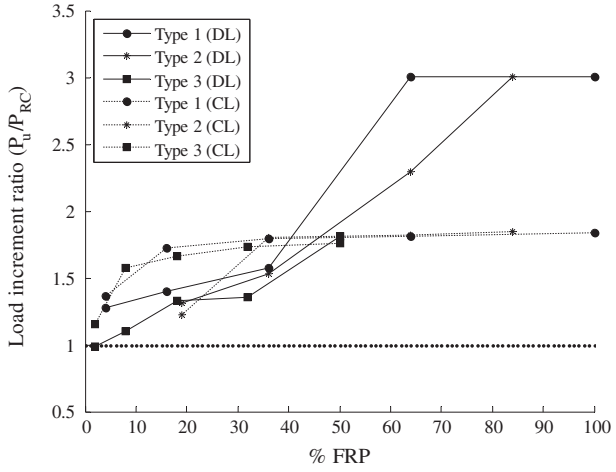

Fig. 10. Load increment ratio in different FRP ratio for $f_c' = 32.87$ MPa, $\rho_s = 0.0037$, and fiber orientation $[90/0]_2$.

2 cases of layers, one FRP layer ($n = 1$) and two FRP layers ($n = 2$). Five different combinations fiber orientations were considered, i.e.: $[0/0]_n$, $[15/-15]_n$, $[30/-30]_n$, $[45/-45]_n$, and $[90/0]_n$. The fiber angle of the lamina is measured counterclockwise from the *X*-axis to the *Y*-axis. For the matrix, three variants of concrete properties, 25 MPa, 32.87 MPa, and 40 MPa, and two variants of steel reinforcement ratio, 0.0037 and 0.01, were examined.

Since *X* and *Y* axes (Fig. 5) are symmetric lines of the plate, only a quarter of plate was modeled and symmetric boundary conditions were placed along the two symmetric planes. The plates' model was exhibited by 25 elements of eight-node quadrilateral shell elements with six degrees of freedom per node while FRP modeled by triangular and quadrilateral shell elements. The FRP shell elements were attached to the tensile surface of the concrete plate directly and perfect bonding between FRP and the concrete was assumed.

4.1. Performance of RC square plate due to subjected load

The numerical analysis initiates with square plate's simulation of the pure RC. The purposes are to evaluate the capacity of the plates in different types of loading. Two conditions are considered: (1) plates that subjected to distributed load and (2) plates that subjected to concentrated load. The plates are modeled with the identical dimension and boundary conditions that refer to Mosallam's experimental works [10]. Two loading pattern are considered, a distributed load that uniformly distributed within entire plate and an equivalent concentrated load at the center of the plates. The results of applied total lateral forces from pure RC plates become baseline for the strengthening cases.

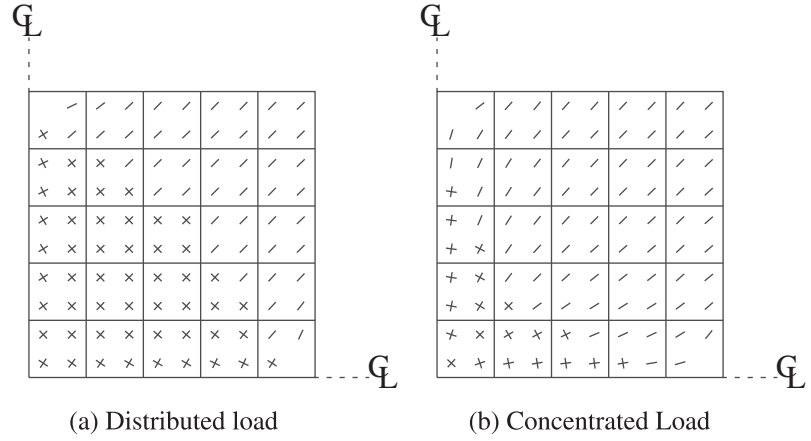

Fig. 11. Crack pattern for composite square plate strengthening by 100% FRP $[90/0]_2$.

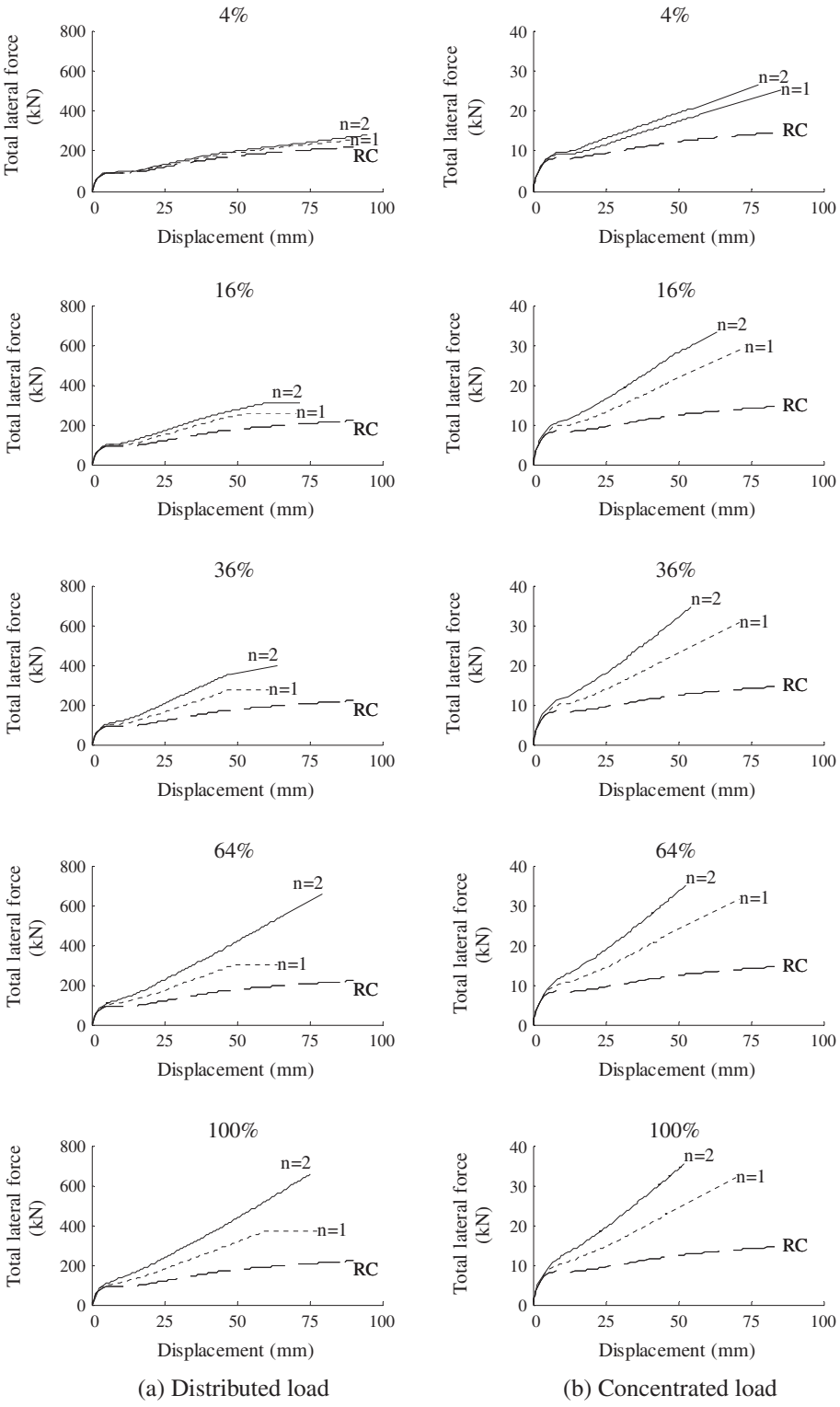

Fig. 12. Type 1 comparison of load–displacement curves in different FRP thicknesses for each FRP ratios with $f'_c = 32.87$ MPa, $\rho_s = 0.0037$ and fiber orientation $[90/0]_n$.

Fig. 6 presents load–displacement curve for the RC plate subjected to distributed load whereas Fig. 8 shows load–displacement curve for the RC plate subjected to concentrated load. The ultimate load for the plate subjected to concentrated load is 13.1 kN. This number is relatively small since only covers approximately 6% from the ultimate load of the plate subjected to distributed load. It is observed in Fig. 9b that local failure only occurs in few elements at the center near the located concentrated load. Once those elements are failed, the entire plate detects as failure. On the other hand, more elements can work to resist the load in the plate subjected to distributed load so that higher total applied load can be resisted. The global failure occurs

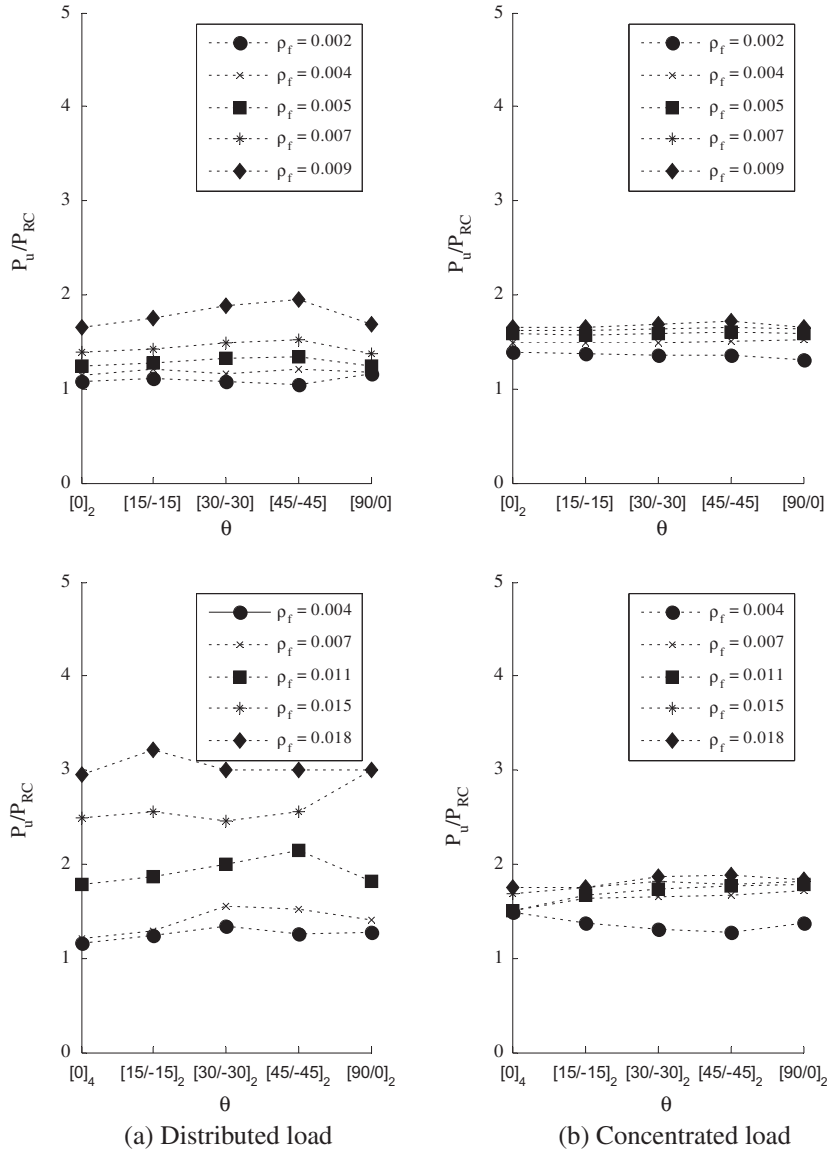

Fig. 13. Load increment ratio in different fiber orientation and FRP reinforcement ratio for $f'_c = 32.87$ MPa and $\rho_s = 0.0037$.

subsequently as many elements act simultaneously resisting the load.

The crack patterns in Fig. 9 demonstrate 45° cracks perform along diagonal of the plate. Comparing Fig. 9a and Fig. 9b, the plate subjected to distributed load has more two directional cracks rather than the plate subjected to concentrated load. This indicates that many elements have fully utilized so that the plate is failed in both directions. On the contrary, only few elements near the center line have cracks in two directions for the plate subjected to concentrated load. This crack pattern can verify that the plate subjected to concentrated load cannot act simultaneously resisting the load so failure of few elements generates failure of the entire plate. Therefore, the ultimate load for the plate subjected to concentrated load is relatively small compare to the plate subjected to distributed load.

4.2. The effect of FRP reinforcements in strengthening composite square plates

This section reports the various factors that may affect the composite plates. First, the plates were tested with three types of strengthening patterns in different area percentage of FRP. The aim is to observe the best location for adhered FRP that will be utilize in further numerical analysis. The analysis continues in examining sufficient FRP ratio within the subjected loading, stimulating number of FRP layers and five combinations of angle laminates. To evaluate the optimum strength of the composite plate, load increment ratios (P_u/P_{RC}) of the total lateral forces are discussed for each case of FRP ratio. P_U is calculated as the maximum value of the total lateral forces for the composite plates while P_{RC} is calculated as the maximum value of the total lateral forces for the pure RC plate.

4.2.1. FRP locations

Fig. 10 illustrates how the modification of FRP shapes and ratios can increase the total lateral load of the composite plates. The similar amount of FRP ratio generates different results of strengthening if the shapes are modified. For plates subjected to distributed load, type 3 gives smaller P_u/P_{RC} than other two cases. The composite plates with 8% FRP in type 3 attain smaller load than 4% FRP in type 1. Type 1 presents the best strengthening effect while type 3 offers the worst pattern results. Considering crack pattern in Fig. 9a

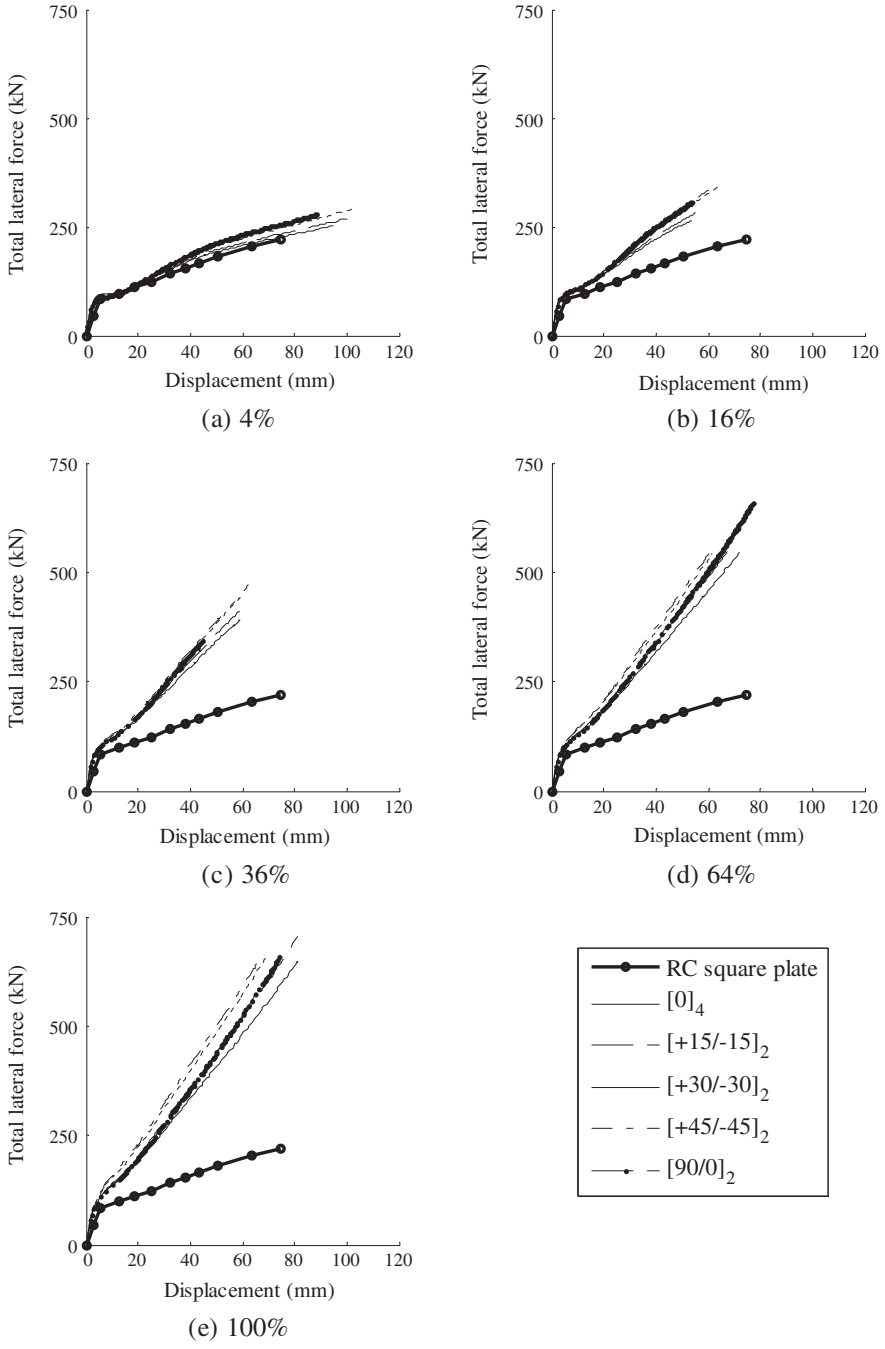

Fig. 14. Comparison of load–displacement curves for type 1 in different FRP percentage and fiber angle of laminates for distributed load for $f'_c = 32.87$ MPa and $\rho_s = 0.0037$.

for pure RC plate, totally 12 elements have two directional cracks. By adhered 36% FRP ratio in type 1, FRPs have covered 75% elements that have two directional cracks, while 36% FRP ratios in type 2 have covered only 42% of the total crack elements. The results indicate the more the FRPs attach to cover the possible crack elements, the higher the results of the P_u/P_{RC}. 50% FRP in type 3 has covered most of the elements that have two directional cracks but actually FRPs only cover half of elements, so that the composite behavior cannot act simultaneously. Accordingly, the cracks still generate a failure for the plates. In general, the P_u/P_{RC} of type 1 is slightly higher than type 2 and type 3.

For composite plates subjected to concentrated load, type 3 presents the best strengthening patterns in lower FRP ratios. Diamond shape in type 3 can enveloped most of the two directional cracks that illustrated in Fig. 9b with lower FRP ratio. However, sufficient percentages of the FRP in type 1 and type 2 generate significant results for strengthened plates. If the plates have been adhered by sufficient percentage of the FRP, P_u/P_{RC} are hardly to be increased. In general, all of the strengthened types produce excellent results for composite plates subjected to concentrated load.

Fig. 11 illustrates the crack pattern for the composite plates that fully adhered by FRP. Comparing Fig. 11a and Fig. 11b, the composite plate that subjected to distributed load appears to have more two directional cracks. More cracks appeared show that most of elements are reached their full strength in order to fully utilize the overall composite behavior. Although the plate has been fully

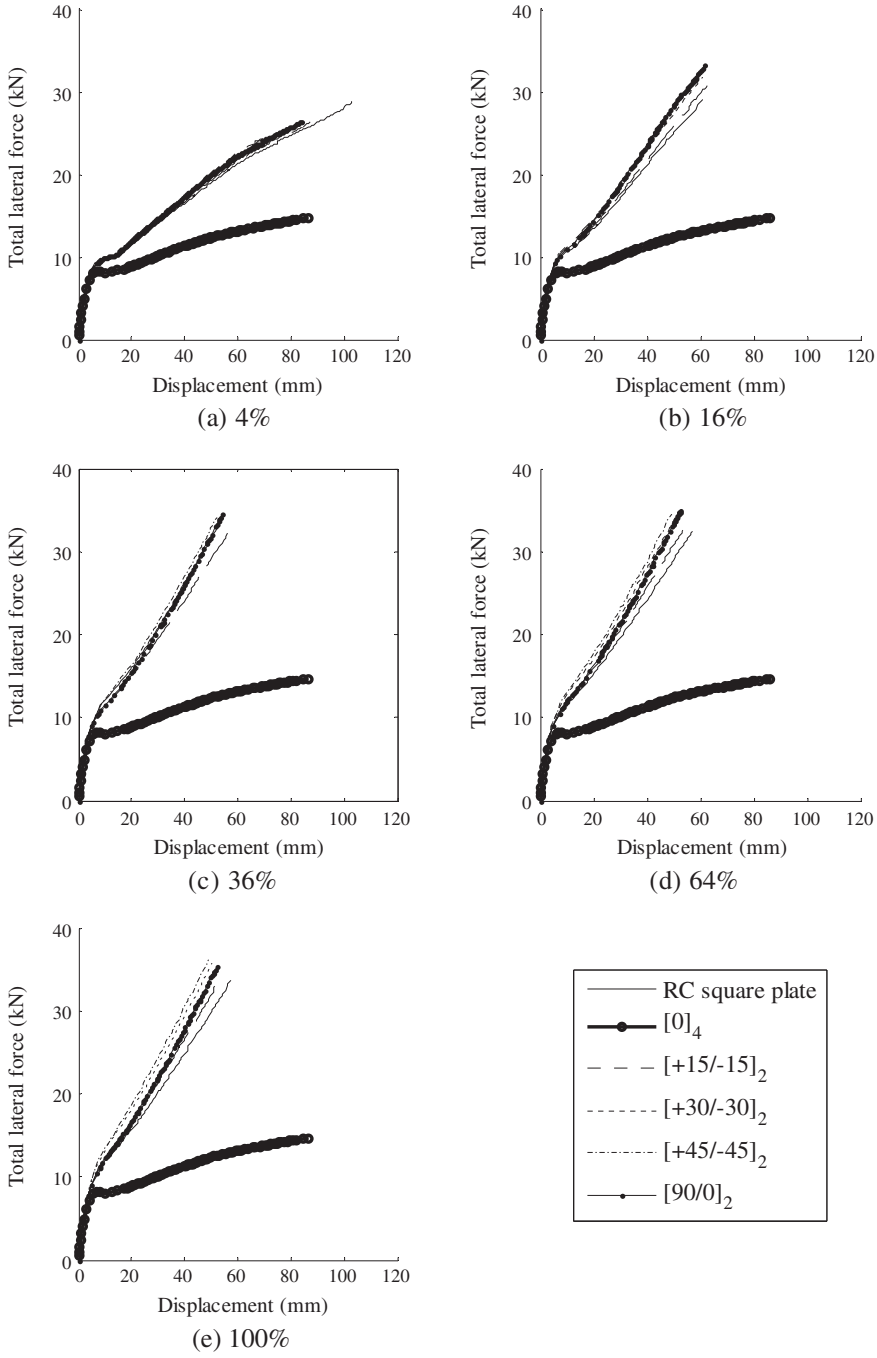

Fig. 15. Comparison of load–displacement curves for type 1 in different FRP percentage and fiber angle of laminates for concentrated load for $f'_c = 32.87$ MPa and $\rho_s = 0.0037$.

adhered by FRP, the crack pattern in Fig. 11b presents few crack transformations compared to pure RC plate in Fig. 9b. Adding higher FRP ratios are inefficient for the plates subjected to concentrated load since the plates only require sufficient FRP ratio around location of the load.

4.2.2. FRP ratios

As the FRP ratios become higher, the average ultimate loads tend to gradually higher. Adhered more FRP can increase the capacity of the composite plates. However, the increment will not significant increased as the sufficient FRPs have been adhered. The results in Fig. 10 shows the composite plates subjected to distributed load can be increased three times the capacity of the pure RC plate. The P_u/P_{RC} of the strengthened plates depends not only on location of FRPs attached but also on how much FRP adhered to the plates. For lower FRP ratios in Fig. 12a 4% and 16%, the curves tend to parallel with pure RC plate which indicate behaviors of the composite plates are dominated by the concrete. In contrast, the curves become more linear once more FRPs are adhered. These patterns demonstrate that behaviors of the composite plates with higher percentage of FRP ratios are controlled by the behavior of carbon FRP. It is noted that the composition of the FRP should be designed carefully to prevent member failure accordingly.

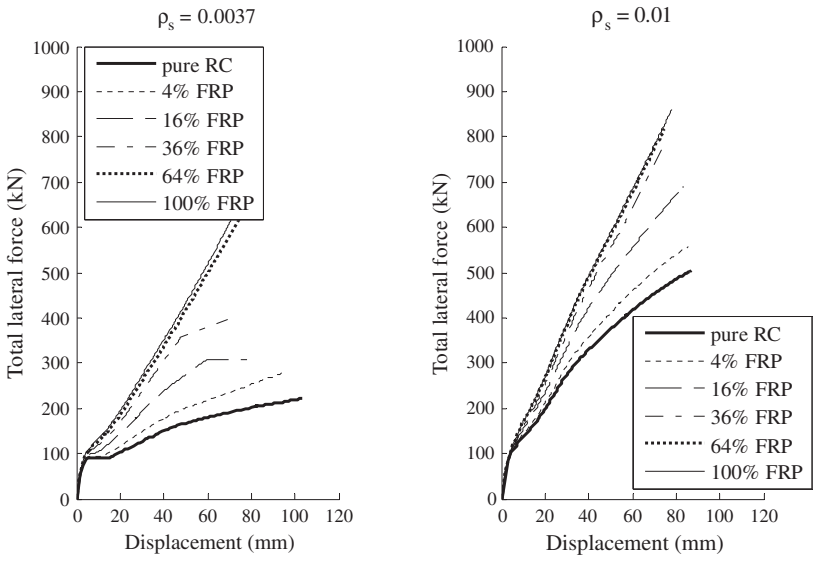

(a) Distributed load

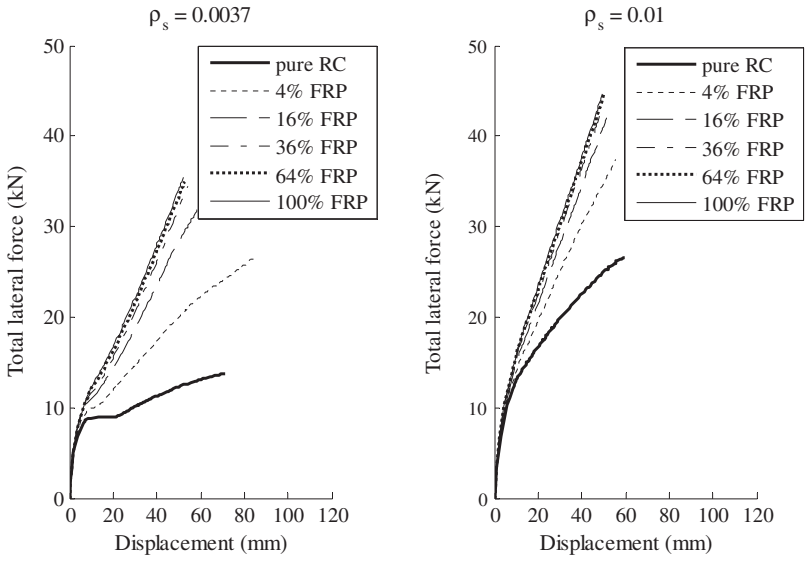

(b) Concentrated load

Fig. 16. Type 1 comparison of load–displacement curves in different steel reinforcement ratio for $f_c' = 32.87$ MPa and FRP fiber orientation $[90/0]_2$.

For the composite plates subjected to concentrated load, Figs. 10 and 12b show adding more FRP areas do not give significant increase to the ultimate load. The maximum average load increment ratio is 1.8. It is clearly shown in Fig. 10 that after the plates have sufficient FRP ratios, adding more FRPs generate similar P_u/P_{RC}. The P_u/P_{RC} significantly increases when FRP ratios are less than 16% for type 1, 36% for type 2 and 8% for type 3. Taking type 1 in Fig. 12b as examples, the ultimate loads for 4%, 16%, 36%, 64%, and 100% FRP ratios are 26.2 kN, 31.5 kN, 32.7 kN, 34.1 kN, and 35 kN, respectively. In this case, the composite plates that adhered 36% FRP have been strengthened adequately. Concentrated load generates extremely failure only in few elements, adding more FRP will not increase the resistant of the composite plates. FRP ratios only affect P_u/P_{RC} until a certain limit of FRP. Local failure is occurred for the plates subjected to concentrated load so that adhered plates with bigger area of FRP will not increase the total applied load since only few elements act simultaneously to resist the load. In addition, engineers need to consider how to provide higher ultimate load with minimum FRP material.

4.2.3. Number of FRP layers

Since type 1 provides better performance in strengthening pure RC plates under both subjected loads, further numerical analyses are only conducted for type 1. This section will examine the effect FRP reinforcement using variation of number of FRP layers, one layer $[\theta_1/\theta_2]_1$ and two layers $[\theta_1/\theta_2]_2$. Fig. 12 demonstrates more FRP layers attain higher ultimate load. When the % FRPs are higher, the effect of number of FRP layers on the ultimate loads will be more significant until a certain limit. For examples, the relative differences between ultimate loads for two layers and one layer are 9.06%, 16.45%, 31.52%, 54.57%, and 43.84% for distributed load,

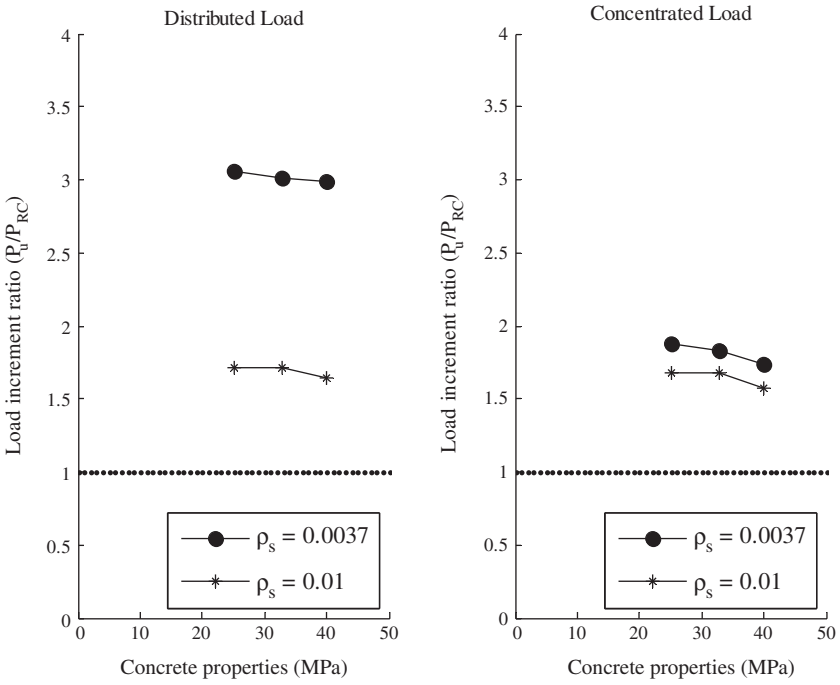

Fig. 17. Type 1 comparison of load increment ratio in different concrete properties and ρ_s for 100% FRP with fiber orientation $[90/0]_2$.

and 4.35%, 11.73%, 10.92%, 9.31%, and 9.56% for concentrated load. Adhered another layers on the plates subjected to distributed load will be more effective compare to the plates subjected to concentrated load. The similar trends can be found with the pervious section that after 16% FRP, adhered more FRP reinforcement will not construct significant increment of the ultimate loads. The increased from one layer to two FRP layers for concentrated load are smaller than for distributed load, which are the increased of FRP layers on concentrated load can be until 12%, while the distributed load can reach until 55%.

Compared one layer and two layers in Fig. 12a and Fig. 12b, the curves subjected to distributed loads become significant stiffer and linear as the FRP ratios and number of layers increase, not like the curves subjected to concentrated loads that the curves tend to be stiff and linear from lower % FRP. Generally, similar trends can be found from composite plates subjected to both loadings. Adhered more layers are equal to adding more FRP reinforcement to composite plates. More FRP reinforcement can strength composite plates until some limit, after that limit more FRP reinforcement will not give significant increment to the ultimate load.

4.2.4. Fiber orientations

Fig. 13a presents P_u/P_{RC} versus five combinations of fiber orientation for type 1 in different FRP reinforcement ratio (ρ_f) for the composite plates subjected to the distributed load, while Fig. 13b for the composite plates subjected to the concentrated load. The FRP reinforcement ratio can be derived as:

$$\rho_f = \frac{A_f}{bd} \tag{27}$$

where total area of FRP (A_f) can be calculated from number of FRP layers (n_f), width of FRP (b_f), and thickness of each FRP layer (t_f), as $A_f = n_f b_f t_f$.

In general, standard deviations of the P_u/P_{RC} for each ρ_f are less than 20%. Different combinations of fiber orientations present similar results of P_u/P_{RC}. The effect of fiber orientation to P_u/P_{RC} is greater for the composite plates subjected to distributed load rather than the plates subjected to distributed load. Since fiber angle orientation of laminates have small influences to the ultimate loads, the combination of $[0/0]_n$ and $[90/0]_n$ are recommended due to simple fabrication and installment.

Considering Fig. 14 and Fig. 15, nonlinear shear of FRP does not appear significant results. For example in Fig. 14e, the curves for [15/−15], [30/−30], and [45/−45] are roughly parallel with $[0]_2$ and [90/0] that implicitly have no nonlinear shear effects. Owing to the small failure shear strain of the composite plates, the material nonlinearity of FRP in in-plane shear stress–strain relation does not have too much influence to the behavior of the composite square plates.

4.3. The effect of steel properties in strengthening composite square plates

Fig. 16 illustrates the ultimate load will significantly increase with the increasing of steel reinforcement ratio (ρ_S). ρ_S can be expressed as:

$$\rho_s = \frac{A_s}{bd} \tag{28}$$

where A_s is total area of rebar, b is the width of the RC plates and d is the equivalent depth of RC plates.

The higher the value of ρ_S, the higher ultimate load and stiffer curve can be obtained. Adding more steel in plates will construct higher ultimate load but lower ductility in return. The curves become more linear as the steel ratios become higher. If the plates without FRP are compared with the plates with FRP, the significant changed of the stiffness show only in lower steel reinforcement ratio. As the ratios increase, the stiffness of the slabs with and without FRP are became coincide. The results for the composite plates with 100% FRP and fiber orientation $[90/0]_2$ as illustrated in Fig. 16 shows the plates with lower ρ_S can be strengthened more than two and half times of the original load, while the plate with higher ρ_S can be strengthened less than two times of the original load. Fig. 17 also presents the P_u/P_{RC}

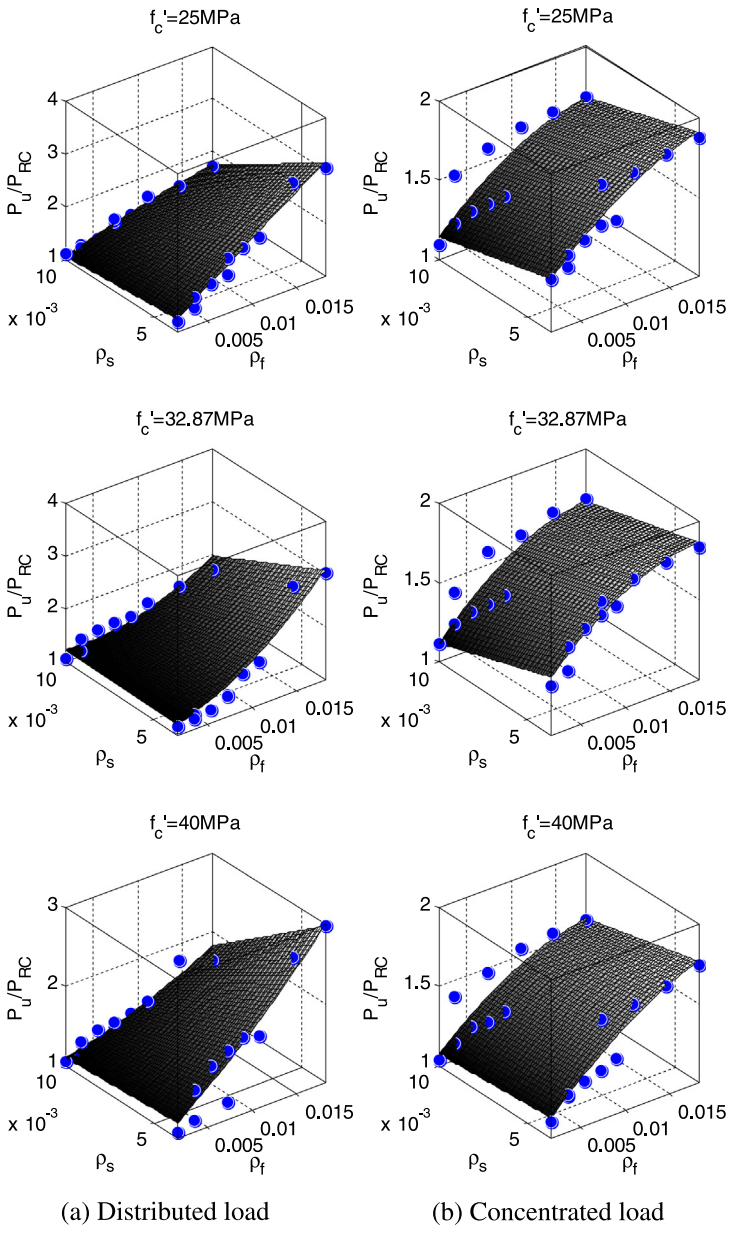

Fig. 18. The effects of f'_c, ρ_s, and ρ_f on the overall behavior of the composite square plates with fiber orientation $[90/0]_2$ (3D plots).

Table 1
Estimation increment of strengthened RC square plates subjected to both loadings.

	Loading	
	Distributed load	Concentrated load
f'_c (MPa)		
25	$P_u/P_{RC} = 1 + 176\rho_f - 4\rho_s - 802\rho_f^2 - 11,810\rho_f\rho_s$	$P_u/P_{RC} = 1 + 64\rho_f - 29\rho_s - 1362\rho_f^2 - 435\rho_f\rho_s$
32.87	$P_u/P_{RC} = 1 + 78\rho_f + 30\rho_s + 3817\rho_f^2 - 11,100\rho_f\rho_s$	$P_u/P_{RC} = 1 + 63\rho_f - 39\rho_s - 1712\rho_f^2 + 455\rho_f\rho_s$
40	$P_u/P_{RC} = 1 + 123\rho_f + 6\rho_s + 1213\rho_f^2 - 10,420\rho_f\rho_s$	$P_u/P_{RC} = 1 + 68\rho_f - 5\rho_s - 1212\rho_f^2 - 1314\rho_f\rho_s$

for $\rho_S = 0.0037$ are greater than the P_u/P_{RC} for $\rho_S = 0.01$. FRP strengthening is more effective for lower steel reinforcement ratio (ρ_S), since FRPs can become the replacement of the tensile strength of the RC.

The P_u/P_{RC} results of the plates with $f'_c = 32.87$ MPa in Fig. 17 are 3 for $\rho_S = 0.0037$ (distributed load), 1.7 for $\rho_S = 0.01$ (distributed load), 1.8 for $\rho_S = 0.0037$ (concentrated load), and 1.7 for $\rho_S = 0.01$ (concentrated load). The relative differences from the

Table 2
The relationship between P_u/P_{RC} and ρ_f for strengthened RC square plates subjected to distributed load in numerous of f_c' and ρ_s.

	ρ_s	
	0.0037	0.0100
f_c' (MPa)		
25	$P_u/P_{RC} = 1 + 132\rho_f - 802\rho_f^2$	$P_u/P_{RC} = 1 + 58\rho_f - 802\rho_f^2$
32.87	$P_u/P_{RC} = 1 + 37\rho_f + 3817\rho_f^2$	$P_u/P_{RC} = 1 - 33\rho_f + 3817\rho_f^2$
40	$P_u/P_{RC} = 1 + 85\rho_f + 1213\rho_f^2$	$P_u/P_{RC} = 1 + 19\rho_f + 1213\rho_f^2$

Table 3
The relationship between P_u/P_{RC} and ρ_f for strengthened RC square plates subjected to distributed load in numerous of f_c' and ρ_s.

	ρ_s	
	0.0037	0.0100
f_c' (MPa)		
25	$P_u/P_{RC} = 1 + 63\rho_f - 1362\rho_f^2$	$P_u/P_{RC} = 1 + 60\rho_f - 1362\rho_f^2$
32.87	$P_u/P_{RC} = 1 + 65\rho_f - 1712\rho_f^2$	$P_u/P_{RC} = 1 + 68\rho_f - 1712\rho_f^2$
40	$P_u/P_{RC} = 1 + 63\rho_f - 1212\rho_f^2$	$P_u/P_{RC} = 1 + 55\rho_f - 1212\rho_f^2$

variation of steel properties are 43.3% (distributed load) and 5.6% (concentrated load). Compared to the plates subjected to concentrated load, the effects of steel properties are significant for the plates subjected to distributed load.

4.4. The effect of concrete properties in strengthening composite square plates

Fig. 17 illustrates some plots for composite plates with 100% FRP and fiber orientation $[90/0]_2$. The standard deviations for variations of the concrete properties are 3.67% ($\rho_S = 0.0037$ distributed load), 4.16% ($\rho_S = 0.01$ distributed load), 7.09% ($\rho_S = 0.0037$ concentrated load), and 5.89% ($\rho_S = 0.01$ concentrated load). The results of standard deviation that less than 10% show the variation of concrete properties generate small influence to the P_u/P_{RC} of the composite plates.

The actual P_{RC} results for the plates subjected to distributed load are 214 kN ($\rho_S = 0.0037$; $f_c' = 25$ MPa), 219 kN ($\rho_S = 0.0037$; $f_c' = 32.87$ MPa), and 240 kN ($\rho_S = 0.0037$; $f_c' = 40$ MPa). The actual P_U results for the plates subjected to distributed load are 655 kN ($\rho_S = 0.0037$; $f_c' = 25$ MPa), 659 kN ($\rho_S = 0.0037$; $f_c' = 32.87$ MPa), and 719 kN ($\rho_S = 0.0037$; $f_c' = 40$ MPa). The results from Fig. 17 for the composite plates under different conditions are similar. The actual P_{RC} and P_U increase with the increasing of f_c'. However, P_u/P_{RC} decreases with the increasing of f_c'. The effect of concrete strength is more pronounced in the pure RC plates rather than the composite plates.

4.5. General behavior of the strengthened square plates

To predict the increment of the ultimate load capacities of the square reinforced concrete plates strengthened by FRPs, empirical equations are proposed based on the numerical results. Fig. 18 presents the curves fitting for composite plates subjected to both loadings. The curves fitting are associated to FRP reinforcement ratio (ρ_f), steel reinforcement ratio (ρ_S) and the load increment ratio (P_u/P_{RC}) for composite plates in various concrete properties (f_c').

The approach between P_u/P_{RC} and ρ_f are represented as quadratic equation, while P_u/P_{RC} and ρ_S are represented as linear equation. The standard error of estimate (SEE) and coefficient of determination (R-square) are used to measure agreement between numerical results and predicted values. A SEE of 0 and R-square of 1 indicate that the fitting perfectly fits the data. For composite plates subjected to distributed load, SEE is 0.21 and R-square is 0.97 for 25 MPa, SEE is 0.67 and R-square is 0.88 for 32.87 MPa, and SEE is 0.60 and R-square is 0.89 for 40 MPa. The fitting can predict the ultimate load capacities perfectly fit the numerical data.

The equations in Table 1 are generated from three dimensional fitting of ρ_f, ρ_S and P_u/P_{RC} from the plates that strengthened by $[90/0]_2$ FRP. If the values of $\rho_S = 0.0037$ and $\rho_S = 0.01$ are included, then the equations can be seen in Table 2 for the plates subjected to distributed load and Table 3 for the plates subjected to concentrated load. The illustrations of those equations are presented in Fig 19. It is clearly shown from the figure that the curves for $\rho_S = 0.0037$ are stiffer than the curves for $\rho_S = 0.01$. These curves show that the strengthening effect is more significant for RC plates under lower steel reinforcement ratio. However, Fig. 19b for composite plates subjected to concentrated load shows that the curves for $\rho_S = 0.0037$ and the curves for $\rho_S = 0.01$ are almost parallel, but as the concrete properties become lower, the curves become more coincide. Similar with the composite plates subjected to distributed load, the strengthening effect is more significant for the plates under lower ρ_S. Those curve plots shows good agreement between numerical results of composite plates subjected to concentrated load and predicted values of the load increment ratio.

5. Conclusions

A rational numerical model that considers appropriate constitutive models has been developed to analyze the reinforced concrete plates strengthened by FRP. The behavior of RC plate and strengthened plate are predicted accurately against the experimental data. The trends of composite plates subjected to distributed load or concentrated load are similar but the ultimate loads are significantly reduced for the plates subjected to concentrated load. In principal, the more FRP are adhered to the composite plates, the higher stiffness and ultimate load capacity can be obtained. However, the significant increment cannot be achieved if all elements that contain two directional cracks have been covered by FRPs. Owing to the small failure shear strain of the composite plates, the material nonlinearity of FRP in in-plane shear stress–strain relation does not have too much influence in the behavior of the composite square plates. The fiber orientation of lamina appears only give a little influence to some cases of FRP ratios, thus, combination of laminates can be assumed to be generalized to simplify the calculation. Increasing number of layers is equal to adding more FRP reinforcement to composite plates. More FRP reinforcement can strength composite plates until some limit, after that limit more FRP reinforcement will not give significant increment to the ultimate load. Concrete properties offer small outcome to the composite plates. Capacity of the composite plates has significant results if more FRP reinforcement is adhered on smaller steel reinforcement ratio RC plates. Finally, the sensitivity studies have been presented to observe the ultimate capacities of the square reinforced concrete plates strengthened by two layer carbon FRP. The detail design should be analyzed carefully before the FRP applied in engineering practices.

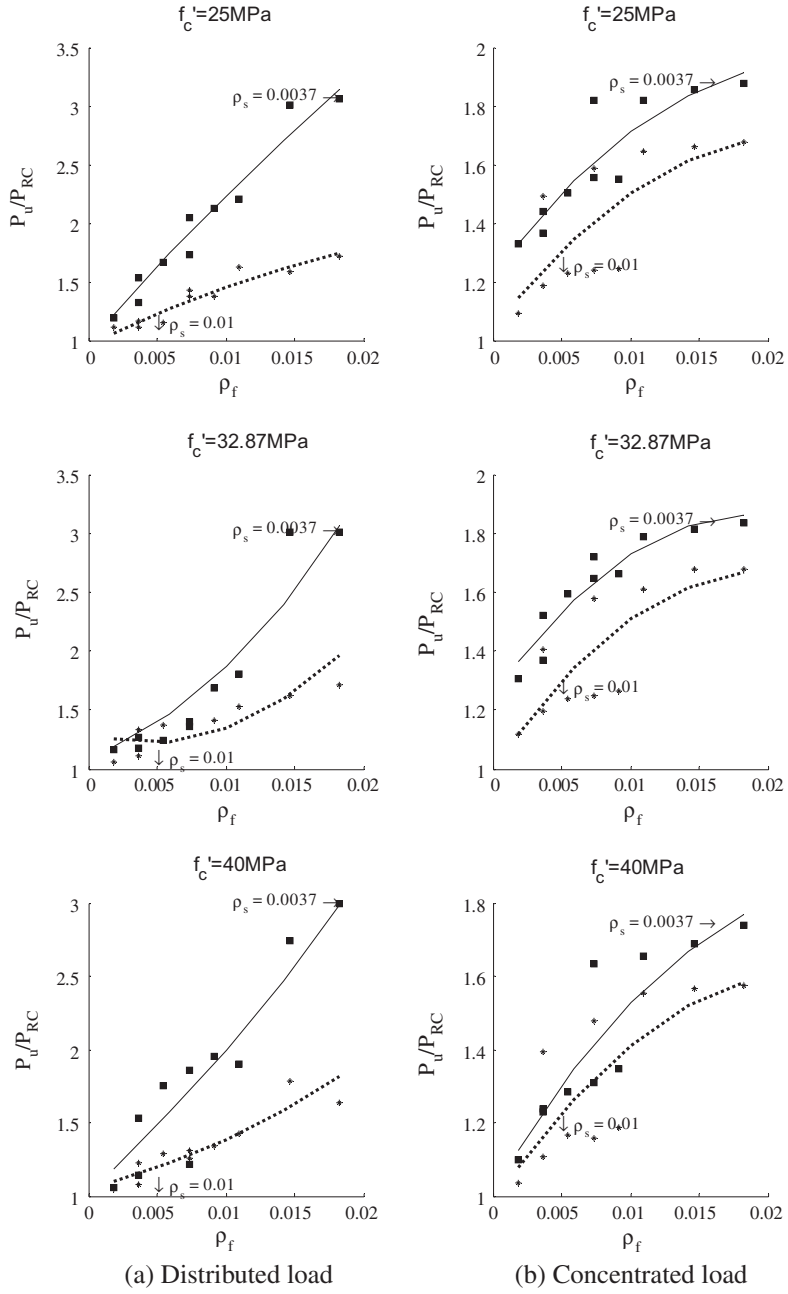

Fig. 19. The effects of f'_c, ρ_s, and ρ_f on the overall behavior of the composite square plates with fiber orientation $[90/0]_2$ (2D plots).

Acknowledgment

This research work was financially supported by the National Science Council, Republic of China under Grant NSC 94-2211-E-006-054.

References

[1] The Concrete Society Technical Report 55. Design guidance for strengthening concrete structures using fibre composite materials. Crowthorne, UK: The Concrete Society; 2000.
[2] Ascione F, Berardi VP, Feo L, Giordano A. An experimental study on the long-term behavior of CFRP pultruded laminates suitable to concrete structures rehabilitation. Compos B: Eng 2008;39(7–8):1147–50.
[3] D'Ambrisi A, Feo L, Focacci F. Experimental analysis on bond between PBO-FRCM strengthening materials and concrete. Compos B: Eng 2012.
[4] D'Ambrisi A, Feo L, Focacci F. Bond-slip relations for PBO-FRCM materials externally bonded to concrete. Compos B: Eng 2012.
[5] Yuan H, Lu X, Hui D, Feo L. Studies on FRP-concrete interface with hardening and softening bond-slip law. Compos Struct 2012;94(12):3781–92.
[6] Al-Sunna R, Pilakoutas K, Hajirasouliha I, Guadagnini M. Deflection behaviour of FRP reinforced concrete beams and slabs: an experimental investigation. Compos B: Eng 2012;43(5):2125–34.
[7] Vougioukas E, Zeris CA, Kotsovos MD. Toward safe and efficient use of fiber-reinforced polymer for repair and strengthening of reinforced concrete structures. ACI Struct J 2005;102(4):525–34.
[8] Ha G-J, Cho C-G, Kang H-W, Feo L. Seismic improvement of RC beam-column joints using hexagonal CFRP bars combined with CFRP sheets. Compos Struct 2012.
[9] Aprile A, Feo L. Concrete cover rip-off of R/C beams strengthened with FRP composites. Compos B: Eng 2007;38(5–6):759–71.
[10] Mosallam AS, Mosalam KM. Strengthening of two-way concrete slabs with FRP composite laminates. Constr Build Mater 2003;17(1):43–54.
[11] Chaallal O, Shahawy M, Hassan M. Performance of axially loaded short rectangular columns strengthened with carbon fiber-reinforced polymer wrapping. J Compos Constr 2003;7(3):200.
[12] Ascione L, Berardi VP, Feo L, Mancusi G. A numerical evaluation of the interlaminar stress state in externally FRP plated RC beams. Compos B: Eng 2005;36(1):83–90.

[13] Hu H-T, Lin F-M, Jan Y-Y. Nonlinear finite element analysis of reinforced concrete beams strengthened by fiber-reinforced plastics. Compos Struct 2004;63(3–4):271–81.
[14] Tedesco JW, Stallings JM, El-Mihilmy M. Finite element method analysis of a concrete bridge repaired with fiber reinforced plastic laminates. Comput Struct 1999;72(1–3):379–407.
[15] Ascione L, Feo L. Modeling of composite/concrete interface of RC beams strengthened with composite laminates. Compos B: Eng 2000;31(6–7):535–40.
[16] Hahn HT, Tsai SW. Nonlinear elastic behavior of unidirectional composite laminae. J Compos Mater 1973;7(1):102–18.
[17] Jones RM, Morgan HS. Analysis of nonlinear stress-strain behavior of fiber-reinforced composite materials. AIAA J 1977;15(12):1669–76.
[18] Hu HT, Lin FM, Liu HT, Huang YF, Pan TC. Constitutive modeling of reinforced concrete and prestressed concrete structures strengthened by fiber-reinforced plastics. Compos Struct 2010;92(7):1640–50.
[19] Abaqus Inc. Abaqus analysis user's manuals and example problems manuals, version 6.11 Providence, Rhode Island; 2011.
[20] ASCE Task Committee on Concrete and Masonry Structure. State of the art report on finite element analysis of reinforced concrete. ASCE; 1982.
[21] ACI Committee 318. Building code requirements for structural concrete and commentary (ACI 318-08). Detroit, Michigan; 2008.
[22] Kupfer H, Hilsdorf HK, Rusch H. Behavior of concrete under biaxial stresses. ACI Struct J 1969;66(8):656–66.
[23] Saenz L. Discussion of "Equation for the stress-strain curve of concrete" by Desayi P, and Krishnan S. ACI Struct J 1964;61(9):1229–35.
[24] Hu HT, Schnobrich WC. Constitutive modeling of concrete by using nonassociated plasticity. J Mater Civil Eng ASCE 1989;1(4):199–216.
[25] Hu H-T, Schnobrich WC. Nonlinear analysis of cracked reinforced concrete. ACI Struct J 1990;87(2):199–207.
[26] Tsai SW, Wu EM. A general theory of strength for anisotropic materials. J Compos Mater 1971;5(1):58–80.
[27] Narayanaswami R, Adelman HM. Evaluation of the tensor polynomial and hoffman strength theories for composite materials. J Compos Mater 1977;11(4):366–77.
[28] Rowlands RE. In: Sih GC, Skudra AM, editors. Strength (Failure) theories and their experimental correlation failure mechanics of composites. The Netherlands: Elsevier Science Publishers; 1985. p. 71–125.
[29] Lin W-P, Hu H-T. Nonlinear analysis of fiber-reinforced composite laminates subjected to uniaxial tensile load. J Compos Mater 2002;36(12):1429–50.
[30] Oh S-H, Kim K-S, Kim C-G. An efficient postbuckling analysis technique for composite stiffened curved panels. Compos Struct 2006;74(3):361–9.